Herschel: the first science highlights

LETTER TO THE EDITOR

Herschel-ATLAS[⋆]: Evolution of the 250 μm luminosity function out to z = 0.5

S. Dye[1], L. Dunne[5], S. Eales[1], D. J. B. Smith[5], A. Amblard[2], R. Auld[1], M. Baes[3], I. K. Baldry[4], S. Bamford[5],
A. W. Blain[31], D. G. Bonfield[6], M. Bremer[33], D. Burgarella[7], S. Buttiglione[8], E. Cameron[9], A. Cava[10],
D. L. Clements[11], A. Cooray[2], S. Croom[12], A. Dariush[1], G. de Zotti[8], S. Driver[13], J. S. Dunlop[24], D. Frayer[14], J. Fritz[3],
Jonathan P. Gardner[30], H. L. Gomez[1], J. Gonzalez-Nuevo[15], D. Herranz[16], D. Hill[13], A. Hopkins[17], E. Ibar[18],
R. J. Ivison[18], M. J. Jarvis[6], D. H. Jones[17], L. Kelvin[13], G. Lagache[19], L. Leeuw[20], J. Liske[21], M. Lopez-Caniego[16],
J. Loveday[22], S. Maddox[5], M. J. Michałowski[24], M. Negrello[23], P. Norberg[24], M. J. Page[32], H. Parkinson[24],
E. Pascale[1], J. A. Peacock[24], M. Pohlen[1], C. Popescu[25], M. Prescott[4], D. Rigopoulou[28], A. Robotham[13], E. Rigby[5],
G. Rodighiero[8], S. Samui[15], D. Scott[34], S. Serjeant[23], R. Sharp[17], B. Sibthorpe[18], P. Temi[20], M. A. Thompson[6],
R. Tuffs[26], I. Valtchanov[27], P. P. van der Werf[29], E. van Kampen[21], and A. Verma[28]

(Affiliations are available in the online edition)

ABSTRACT

We have determined the luminosity function of 250 μm-selected galaxies detected in the ∼14 deg² science demonstration region of the *Herschel*-ATLAS project out to a redshift of $z = 0.5$. Our findings very clearly show that the luminosity function evolves steadily out to this redshift. By selecting a sub-group of sources within a fixed luminosity interval where incompleteness effects are minimal, we have measured a smooth increase in the comoving 250 μm luminosity density out to $z = 0.2$ where it is $3.6^{+1.4}_{-0.9}$ times higher than the local value.

1. Introduction

Measurement of the galaxy luminosity function (LF) constitutes one of the most fundamental statistical constraints that can be placed on models of galaxy formation, and hence the build up of large scale structure, in the universe. Since half of the energy ever emitted by galaxies has been absorbed by dust and re-radiated at far-infrared and sub-millimetre (submm) wavelengths (Fixsen et al. 1998) and, because knowledge of the statistical properties of submm sources is relatively sparse, determination of the submm LF provides a crucial missing piece in a fully comprehensive model of galaxy evolution.

Following their detection in the first deep submm and mm surveys (e.g., Smail et al. 1997; Hughes et al. 1998; Eales et al. 1999; Bertoldi et al. 2000), much has been learned about the dusty high-redshift sources selected at such wavelengths. Although many studies have argued that these sources are likely ancestors of local ellipticals (e.g., Scott et al. 2002; Dunne et al. 2003) little progress in verifying this assertion has been made since. The main reason for this is the preponderance of high red-shift submm/mm-selected sources, owing to the strong negative k-correction and small survey areas. The resulting low numbers of sources at redshifts $z < 1$ has therefore precluded evolutionary studies over the last ∼60% of the Universe's history.

In particular, despite the local submm LF being first determined a decade ago (Dunne et al. 2000), little has been added to our comprehension of how the LF has evolved over the last ∼7 Gyr, until very recently. Observations conducted using the Balloon-borne Large Aperture Submm Telescope (BLAST; Devlin et al. 2009) have made significant improvements with much enhanced sensitivity to $z < 1$ sources. As a result, direct estimates of the LF at 250, 350 and 500 μm were made by Eales et al. (2009) who detected strong evolution, particularly among the higher luminosity systems, from $z = 1$ to the present day. However, the accuracy of these findings is limited by the small number of sources used (∼50 at $z < 0.5$) and source confusion due to the angular resolution of BLAST.

In this letter, we present our measurement of the LF of 250 μm-selected galaxies detected by the *Herschel* Space Observatory (*Herschel*; Pilbratt et al. 2010) over a ∼14 deg² region acquired as part of the science demonstration observations of the *Herschel*-Astrophysical Terahertz Large Area Survey (H-ATLAS; Eales et al. 2010). These data offer a significant improvement over the BLAST data in terms of their increased sensitivity, higher angular resolution and greater areal coverage, resulting in ∼20 times the number of sources with which to compute the LF.

We have adopted the following cosmological parameters in this letter; $H_0 = 71$ km s^{-1} Mpc^{-1}, $\Omega_m = 0.27$ and $\Omega_\Lambda = 0.73$.

2. Data

The $4° \times 4°$ H-ATLAS science demonstration field was observed with the Spectral and Photometric Imaging REceiver (SPIRE; Griffin et al. 2010) at the wavelengths 250, 350 and 500 μm and with the Photodetector Array Camera and Spectrometer (PACS; Poglitsch et al. 2010) at 100 and 160 μm. The field, centred at the co-ordinates ($09^h05^m30^s$, $+00°30'00''$), was scanned twice in parallel mode. The 5σ point source sensitivities of the resulting beam-convolved maps, including confusion noise, are 132, 126, 32, 36 and 45 mJy and the beam sizes expressed as full width at half maximum (*FWHM*) are 9″, 13″, 18″, 25″ and 35″ at 100, 160, 250, 350 and 500 μm respectively. Details of the SPIRE and PACS map-making are given in Pascale et al. (in prep.) and Ibar et al. (in prep.) respectively.

Sources were initially extracted from the 250 μm noise-weighted beam-convolved map in a central 14.4 deg^2 region above a significance of 2.5σ. For each source, 350 and 500 μm fluxes were then estimated from the appropriate beam-convolved map at positions determined at 250 μm. Extended source fluxes were measured in apertures matched to identified (IDed) optical counterpart sizes (see below). 6878 sources were detected with a significance of $\geq 5\sigma$ in any one band. Fluxes at 100 and 160 μm were assigned by matching to $\geq 3\sigma$ PACS sources within a positional tolerance of 10″. The analysis described hereafter applies to the 6613 sources detected at $\geq 5\sigma$ at 250 μm. Full details of the source extraction are given in Rigby et al. (in prep.).

Since our field (and H-ATLAS at large) is lacking in the radio and mid-infrared data traditionally used to identify counterparts to submm sources, we have taken a different approach and matched directly to optical counterparts. It is possible to attain a reasonable rate of secure optical IDs in this way with H-ATLAS because, unlike existing submm surveys at 850 μm-1.1 mm, sensitive to high redshift sources ($z_{median} \simeq 2.5$), H-ATLAS sources lie at substantially lower redshifts ($z_{median} < 1.0$) on average. This means that we can use shallow optical imaging, where a low surface number density of sources allows for much less ambiguous IDs.

We used the likelihood ratio (LR) method of Sutherland & Saunders (1992) to perform the matching, which uses the submm positional uncertainties and the magnitude distribution of counterparts to assign the likelihood that a particular optical source is physically associated with a target submm galaxy. We searched for optical counterparts at $r \leq 22.4$ from the Sloan Digital Sky Survey (SDSS) seventh data release (Abazajian et al. 2009) within 10″ of every 250 μm SPIRE source. The LR technique assigns a reliability parameter, R_{LR}, to each match, which indicates the probability that the counterpart is the correct ID. The calculation of R_{LR} includes the probability that the true counterpart may be below the detection limit of the survey and accounts for other counterparts within the same search radius. To remove unreliable counterparts, all those with $R_{LR} < 80\%$ were discarded, leaving a total of 2267 submm sources with unique optical counterparts. We refer the reader to Smith et al. (in prep.) for an exhaustive account of the ID procedure.

Of these 2267 counterparts, 876 have spectroscopic redshifts (spec-zs) acquired either by the SDSS, the Galaxy And Mass Assembly survey (Driver et al. 2009), the 2dF redshift survey (Colless et al. 2001) or the 6dF redshift survey (Jones et al. 2009). For the remaining counterparts, photometric redshifts (photo-zs) were estimated by applying the ANNz neural network code (Collister & Lahav 2004) to the SDSS optical photometry and also near-infrared photometry taken from the seventh data release of the UKIRT Infrared Deep Sky Survey
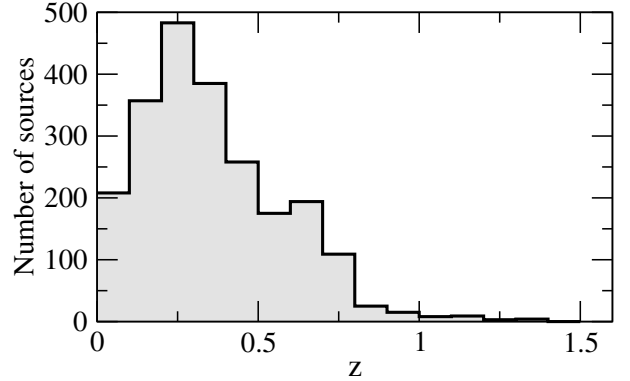
Fig. 1. Redshift distribution of the 2241 sources that are detected at 250 μm with $\geq 5\sigma$ significance, and have an optical counterpart with a redshift and a reliability of association of $\geq 80\%$. The 1688 of these at $z \leq 0.5$ form the sample analysed in this letter.

(UKIDSS; Lawrence et al. 2007). Details of these photo-zs are given in Smith et al. (in prep.). A total of 2239 sources were assigned photo-zs, with a total of 2241 sources having a redshift of either type. Figure 1 shows the redshift distribution of these 2241 sources. The 1688 sources at $z \leq 0.5$ form the sample to which we apply our analysis in this letter. In every case, we used a spec-z in preference to a photo-z, although there is excellent agreement between the two, with a standard deviation of $(z_{phot} - z_{spec})/(1 + z_{spec})$ of 0.039 over the sample.

3. The luminosity function
3.1. SED fitting

A modified black-body spectral energy distribution (SED) was fitted to the SPIRE photometry, and, where available (272 sources), PACS photometry, for each source. In the fitting, we allowed the rest-frame dust temperature, T, to vary between 10 K $< T <$ 50 K, we fixed the dust emissivity index to $\beta = 1.5$ and we fixed the redshift to either the photo-z, or, preferentially, when available, the spec-z. The temperature of 342 sources (none with PACS photometry) could not be reliably constrained. For these, we re-fitted the SED, fixing the temperature to the median of the sample (see below).

Excluding the sources where T was fixed, we found a median dust temperature across the whole sample of 26 K with a standard deviation of 8 K (or 23 ± 7 K for $\beta = 2$). This result closely agrees with the rest-frame dust temperatures determined for BLAST sources measured by Dye et al. (2009) as well as those of the sample of H-ATLAS galaxies studied in Amblard et al. (2010; see also other temperature comparisons therein).

For each source, we measured the rest-frame 250 μm luminosity, L_{250}, by integrating the rest-frame SED over the 250 μm SPIRE bandpass function. Errors on L_{250} were determined by propagating redshift errors and temperature errors obtained from the SED fit.

3.2. Estimating the LF

We based our measurement of the LF on the estimator

$$\phi = \Sigma_i (V_{max,i})^{-1}, \tag{1}$$

where $V_{max,i}$ is the comoving volume out to the maximum redshift that source i could be placed and remain above the 250 μm *and* optical r-band detection threshold. We used an Sb type SED for the optical k-correction and the source-specific SED fit as described in the previous section for the k-correction at 250 μm.
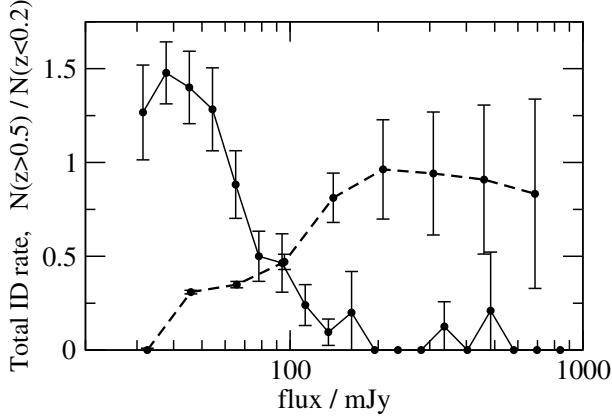
Fig. 2. Rate of identification of optical counterparts to 250 µm sources (dashed line) and ratio of the number of $z > 0.5$ sources to the number of $z < 0.2$ sources (continuous line), as a function of 250 µm flux. Both quantities were determined using the sample of 2241 counterparts. Poisson errors are plotted.

The sum here acts over all sources in a given luminosity and redshift bin. We computed the total error on ϕ as the quadrature sum of its formal error, $\sqrt{\Sigma_i (V_{max,i})^{-2}}$, and the standard deviation of the scatter measured in each bin in performing a Monte Carlo simulation in which redshifts and photometry were randomised according to their errors.

An important consideration when computing the LF is incompleteness. There are two types of incompleteness at play in our case. Firstly, 250 µm sources with optical fluxes lower than the r-band detection threshold are missing. This is a stronger effect at higher redshifts and lower luminosities. Figure 2 shows how the ID rate (i.e., identifying with an optical counterpart with $R_{LR} > 80\%$) varies with 250 µm flux over the full sample of 6613 sources detected at 250 µm. The figure also shows that the ratio of the number of $z > 0.5$ sources to the number of $z < 0.2$ sources[1] increases rapidly towards low 250 µm fluxes. Together, these two facts imply that the unidentified 250 µm sources predominantly lie at high redshifts where their optical flux falls beneath the sensitivity limit of the counterpart catalogue.

However, the fraction of missing sources at $z < 0.5$ (where we have computed the LF – see Sect. 4.1) with undetected optical flux must still be quantified and accounted for. We therefore plotted the optical r-band flux against 250 µm flux for sources in different redshift slices and found a clear positive correlation in every slice. At redshifts $z \gtrsim 0.2$, the faint end of the locus of points on this plot becomes cut by the optical sensitivity limit. Using this result, we were able to determine a 250 µm flux limit for each redshift slice where we estimate that <5% of sources are missing due to the optical sensitivity. We then limited our computation of the LF in each redshift bin by the corresponding 250 µm luminosity limit, ensuring >95% completeness at all redshifts. H-ATLAS completeness effects will be discussed at length in forthcoming work, including Rigby et al. (in prep.).

The second incompleteness effect is a consequence of the reliability cut. Approximately one half of the 250 µm sources that were matched to an optical source, were rejected by applying a minimum reliability of 80%. A certain fraction of these will be genuine counterparts. To estimate this fraction, we applied a correction factor. This factor was computed by reversing the algorithm used in the ID procedure (see Smith et al., in prep.)

---

[1] These two redshift limits were chosen to obtain approximately equally sized sub-samples.

that determines a counterpart's reliability from the radial offset between the submm and optical positions, the optical r-band magnitude and the signal-to-noise ratio of the submm source. We therefore computed the submm-optical offset, r_{80}, corresponding to a reliability of 80% for the full range of combinations of 250 µm source signal-to-noise ratio and r-band magnitude seen in the data. For each combination, the correction factor, c, was then calculated as the reciprocal of the fraction of counterparts that would be IDed within an offset of the smaller of r_{80} and the ID search radius of 10″, i.e.,

$$c = A \left(\int_0^{\min(r_{80}, 10'')} r \exp\left(-\frac{r^2}{2\sigma^2}\right) dr \right)^{-1}, \qquad (2)$$

where the normalisation A is set such that one would obtain $c = 1$ were the integral evaluated between 0 and ∞. Here, σ depends on the submm signal-to-noise, μ, and the beam *FWHM* according to $\sigma = 0.6 * FWHM/\mu$, as given by Ivison et al. (2007). At 250 µm, σ therefore varies from ~2.2″ for a source with $\mu = 5$ to ~1.1″ for a source with $\mu = 10$. These values are consistent with the distribution of offsets obtained in matching to the SDSS. The minimum allowed value of σ was set to 1.0″, to account for the SPIRE pointing error and map pixel size (see Smith et al., in prep., for more details).

The resulting correction factor was then applied by modifying the LF estimator to $\Sigma_i c_i (V_{max,i})^{-1}$ where c_i is the correction factor corresponding to the ith source's 250 µm signal-to-noise and r band counterpart magnitude. The average correction factor, weighted by the counterpart number counts, ranges from ~1.2 for 5σ 250 µm sources, through ~1.1 for 8σ sources to ~1.0 for 10σ sources.

Finally, we estimated the expected number of false counterparts by summing the quantity $1 - R_{LR}$. Within the 1688 sources at $z \leq 0.5$ used for computation of our LF, we estimate a total of 81 false counterparts. This false ID rate of ~5% shows no noticable correlation with redshift or luminosity and little variation between LF bins across the redshift-luminosity plane. We treated the false counterpart rate as an additional source of error and added it in quadrature to the error on each LF bin.
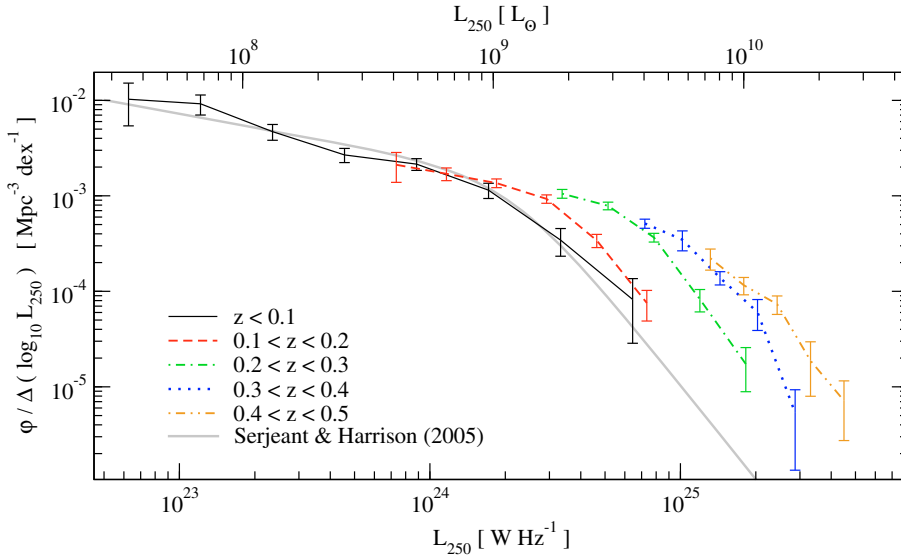
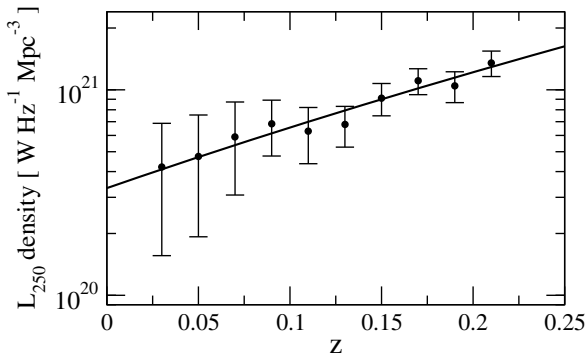## 4. Results
4.1. LF evolution

Using the methods outlined previously, we determined the LF in five redshift bins of width $\Delta z = 0.1$ from $z = 0$ to $z = 0.5$. The total error budget includes the formal error on the LF estimator that accounts for Poisson noise, false IDs and the scatter measured in the Monte Carlo simulation which randomises redshift and photometry.

Figure 3 shows the LF in each of the five redshift bins. The figure clearly shows that the LF exhibits significant evolution out to $z = 0.5$. At a given luminosity, the comoving space density increases steadily with redshift. This is consistent with the findings of Eales et al. (2009), although our detection of evolution is considerably more significant. The figure also shows that the local 250 µm LF predicted by Serjeant & Harrison (2005) agrees very well with our $z < 0.1$ LF.

In each redshift bin, the slope of the LF becomes shallower toward lower luminosities. Our allowed incompleteness of up to 5% is insufficient to account for the magnitude of this effect, although it is possible that there may be additional mild incompleteness in the source extraction process at low 250 µm fluxes. This will be quantified in a later paper once the source extraction has been formally characterised (Rigby et al., in prep.).

Fig. 4. Evolution of comoving rest-frame 250 μm luminosity density out to $z \simeq 0.2$ for sources with luminosity in the range $10^9 < L_{250}/L_\odot < 5 \times 10^9$. Errors were determined using a Monte Carlo simulation which randomised redshifts and photometry and account for Poisson noise. The line is the fit $(1 + z)^{7.1}$.

4.2. Luminosity density evolution

Having established significant evolution of the LF, we investigated evolution of the comoving luminosity density. Clearly, incompleteness will preclude an accurate measurement out to any significant redshift. However, by limiting the calculation to a sub-group of sources within a fixed luminosity interval where incompleteness is small, it is possible to estimate the strength of evolution in the sub-group over a larger redshift range.

We therefore computed the comoving rest-frame 250 μm luminosity density of a sub-group of sources with luminosities in the range $10^9 < L_{250}/L_\odot < 5 \times 10^9$, allowing measurement up to $z \simeq 0.2$ before incompleteness becomes significant. We note that within this luminosity and redshift range, approximately 85% of the sources have spectroscopic redshifts with negligible errors. Figure 4 shows the results. The luminosity density exhibits a steady and significant increase with redshift, which when fit with the form $(1 + z)^n$ yields a value of $n = 7.1^{+2.1}_{-1.4}$. This corresponds to an increase in luminosity density by a factor of $3.6^{+1.4}_{-0.9}$ from the present day to a redshift of $z = 0.2$. This scaling is consistent with Saunders et al. (1990) who measured a density scaling of $(1+z)^{6.7\pm2.3}$ out to $z = 0.25$ for 60 μm-selected galaxies but stronger than the scaling $(1 + z)^{3.9\pm0.7}$ measured by Le Floc'h et al. (2005) to $z \sim 1$ for 24 μm-selected galaxies.

5. Conclusion

One of the key goals of H-ATLAS will be to understand the nature of the evolution detected in this letter. In turn, we aim to improve our understanding of the evolutionary link between high redshift and local submm systems.

This letter has only considered sources selected at 250 μm, merely one of the five wavebands on offer from H-ATLAS. Furthermore, the 14 deg² of survey data analysed in this work represent only 2.5% of the final H-ATLAS survey area. A repeat of the analysis presented here with the final survey data, would therefore result in the quoted uncertainties falling by at least a factor of five. In light of these considerations, it is clear that our results offer only a small glimpse of the anticipated wealth of science that H-ATLAS has to offer.

References

Abazajian, K. N., Adelman-McCarthy, J. K., Agüeros, M. A., et al. 2009, ApJS, 182, 543
Amblard, A., et al. 2010, A&A, 518, L9
Bertoldi, F., Carilli, C. L., Menten, K. M., et al. 2000, A&A, 360, 92
Colless, M. M., Dalton, G. B., Maddox, S. J., et al. 2001, MNRAS, 328, 1039
Collister, A. A., & Lahav, O. 2004, PASP, 116, 345
Devlin, M. J., Ade, P. A. R., Aretxaga, I., et al. 2009, Nature, 458, 737
Driver, S. P., Norberg, P., Baldry, I. K., et al. 2009, A&G, 50, 12
Dunne, L., Eales, S. A., Edmunds, M. G., et al. 2000, MNRAS, 315, 115
Dunne, L., Eales, S. A., & Edmunds, M. G. 2003, MNRAS, 341, 589
Dye, S., Ade, P. A. R., Bock, J. J., et al. 2009, ApJ, 703, 285
Eales, S. A., Lilly, S., Gear, W., et al. 1999, ApJ, 515, 518
Eales, S. A., Chapin, E. L., Devlin, M. J., et al. 2009, ApJ, 707, 1779
Eales, S. A., Dunne, L., Clements, D., et al. 2010, PASP, 122, 499
Fixsen, D. J., Dwek, E., Mather, J. C., Bennet, C. L., & Shafer, R. A. 1998, ApJ, 508, 123
Griffin, M. J., et al. 2010, A&A, 518, L3
Hughes, D. H., Serjeant, S., Dunlop, J. S., et al. 1998, Nature, 394, 241
Ivison, R. J., Greve, T. R., Dunlop, J. S., et al. 2007, MNRAS, 380, 199
Jones, D. H., Read, M. A., Saunders, W., et al. 2009, MNRAS, 399, 683
Lawrence, A., Warren, S. J., Almaini, O., et al. 2007, MNRAS, 379, 1599
Le Floc'h, E., Papovich, C., Dole, H., et al. 2005, ApJ, 632, 169
Pilbratt, G. L., et al. 2010, A&A, 518, L1
Poglitsch, A., et al. 2010, A&A, 518, L2
Saunders, W., Rowan-Robinson, M., & Lawrence, A. 1990, MNRAS, 242, 318
Scott, S. E., Fox, M. J., Dunlop, J. S., et al. 2002, MNRAS, 331, 817
Serjeant, S., & Harrison, D. 2005, MNRAS, 356, 192
Smail, I., Ivison, R. J., & Blain, A. W. 1997, ApJ, 490, L5
Sutherland, W., & Saunders, W. 1992, MNRAS, 259, 413

[1] School of Physics and Astronomy, Cardiff University, Queens Buildings, The Parade, Cardiff, CF24 3AA, UK
e-mail: s.dye@astro.cf.ac.uk

[2] Dept. of Physics & Astronomy, University of California, Irvine, CA 92697, USA

[3] Sterrenkundig Observatorium, Universiteit Gent, Krijgslaan 281 S9, 9000 Gent, Belgium

[4] Astrophysics Research Inst., Liverpool John Moores University, 12 Quays House, Egerton Wharf, Birkenhead, CH41 1LD, UK

[5] School of Physics and Astronomy, University of Nottingham, University Park, Nottingham NG7 2RD, UK

[6] Centre for Astrophysics Research, Science and Technology Research Institute, University of Hertfordshire, Herts AL10 9AB, UK

[7] Laboratoire d'Astrophysique de Marseille, UMR6110 CNRS, 38 rue F. Joliot-Curie, 13388 Marseille, France

[8] University of Padova, Department of Astronomy, Vicolo Osservatorio 3, 35122 Padova, Italy

[9] ETH Zurich, Insitute for Astronomy, HIT J12.3, 8093 Zurich, Switzerland

[10] Instituto de Astrofísica de Canarias (IAC) and Departamento de Astrofísica, Universidad de La Laguna (ULL), La Laguna, Tenerife, Spain

[11] Astrophysics Group, Imperial College, Blackett Laboratory, Prince Consort Road, London SW7 2AZ, UK

[12] Sydney Institute for Astronomy, School of Physics, University of Sydney, NSW 2006, Australia

[13] SUPA, School of Physics and Astronomy, University of St. Andrews, North Haugh, St. Andrews, KY16 9SS, UK

[14] National Radio Astronomy Observatory, PO Box 2, Green Bank, WV 24944, USA

[15] Scuola Internazionale Superiore di Studi Avanzati, via Beirut 2-4, 34151 Triest, Italy

[16] Instituto de Física de Cantabria (CSIC-UC), Santander, 39005, Spain

[17] Anglo-Australian Observatory, PO Box 296, Epping, NSW 1710, Australia

[18] UK Astronomy Technology Center, Royal Observatory, Edinburgh, EH9 3HJ, UK

[19] Institut d'Astrophysique Spatiale, Bâtiment 121, 91405 Orsay, France; Université Paris-Sud 11 and CNRS (UMR 8617), France

[20] Astrophysics Branch, NASA Ames Research Center, Mail Stop 245-6, Moffett Field, CA 94035, USA

[21] European Southern Observatory, Karl-Schwarzschild-Strasse 2 85748, Garching bei Munchen, Germany

[22] Astronomy Centre, Department of Physics and Astronomy, School of Maths and Physical Sciences, Pevensey II Building, University of Sussex, Falmer, Brighton, BN1 9QH, UK

[23] Dept. of Physics and Astronomy, The Open University, Milton Keynes, MK7 6AA, UK

[24] SUPA, Institute for Astronomy, University of Edinburgh, Royal Observatory, Blackford Hill, Edinburgh EH9 3HJ, UK

[25] Jeremiah Horrocks Institute, University of Central Lancashire, Preston PR1 2HE, UK

[26] Max Planck Institute for Nuclear Astrophysics (MPIK), Saupfercheckweg 1, 69117 Heidelberg, Germany

[27] *Herschel* Science Centre, ESAC, ESA, PO Box 78, Villanueva de la Cañada, 28691 Madrid, Spain

[28] Oxford Astrophysics, Denys Wilkinson Building, University of Oxford, Keble Road, Oxford, OX1 3RH, UK

[29] Leiden Observatory, Leiden University, PO Box 9513, 2300 RA Leiden, The Netherlands

[30] Astrophysics Science Division, Observational Cosmology Laboratory, Code 665, Goddard Space Flight Center, Greenbelt, MD 20771, USA

[31] Caltech, MS247-19, Pasadena, CA 91125, USA

[32] University College London, Mullard Space Science Laboratory, Holmbury St. Mary, Dorking, Surrey, RH5 6NT, UK

[33] H H Wills Physics Laboratory, University of Bristol, Tyndall Avenue, Bristol, BS8 1TL, UK

[34] Department of Physics & Astronomy, University of British Columbia, Vancouver, BC, V6T 1Z1, Canada